Z. Phys. Chem. **227** (2013) 901–915 / **DOI** 10.1524/zpch.2013.0398

Immobilization and Characterization of $RuCl_2(PPh_3)_3$ Mesoporous Silica SBA-3

By Anna Grünberg, Torsten Gutmann, Niels Rothermel, Xu Yeping, Hergen Breitzke, and Gerd Buntkowsky*

Eduard-Zintl-Institut für Anorganische und Physikalische Chemie, Technische Universität Darmstadt, Petersenstr. 20, D-64287 Darmstadt, Germany

Dedicated to Prof. Dr. Hans-Heinrich Limbach on the occasion of his 70th birthday

(Received February 5, 2013; accepted in revised form April 8, 2013)
(Published online June 3, 2013)

$RuCl_2(PPh_3)_3$ / Heterogeneous Catalysis / Solid-State-NMR / MAS / Scalar Interactions / Quantum-chemical Calculations

The five-fold coordinated ruthenium (II) catalyst $RuCl_2(PPh_3)_3$ is heterogenized on the surface of amine functionalized mesoporous silica material SBA-3 and studied by BET, XRD and ^{31}P CP-MAS solid-state NMR. The spectra indicate the replacement of one or two of the triphenyl-phosphine groups in the course of the grafting. To distinguish between both possibilities two-dimensional J-resolved ^{31}P MAS solid-state NMR combined with quantum chemical calculations is employed. The changes of the scalar coupling pattern between the neat catalyst and the immobilized catalyst suggest the replacement of two of the PPh_3-groups by coordinative bonds to the amine-functions of the linker. DFT calculations reveal the absence of two chemically and magnetically equivalent phosphines and confirm the replacement of two PPh_3-groups. This finding is similar to the results observed for the binding of the rhodium in the Wilkinson's catalyst, despite the different coordination of the metals (four-fold *versus* five-fold), the presence of two chlorine ligands and the different transition metal.

1. Introduction

Homogeneous organometallic catalysts in solution found applications in many organic reactions like pharmaceutical and natural products chemistry and fine synthesis. Due to the uniqueness of their structure they often combine high activity and selectivity. However, the separation of the catalyst from the products and its recovery is often not easy. This may increase the costs of production and might lead in the worst case to heavy metal pollution of the environment. The latter problems are easily solvable by solid heterogeneous catalysts since they can be very easily separated from the reaction mix-

* Corresponding author. E-mail: gerd.buntkowsky@chemie.tu-darmstadt.de

ture and reused. This gives them big advantages in practical applications and is of great importance for the principles of green chemistry [1]. On the other hand, in many heterogeneous catalysts there is a non-uniform distribution of active sites, causing a broad spectrum of reactivities and low catalytic selectivities [2].

Thus, in recent years strong efforts have been devoted to the development of new supported catalysts with catalytic groups that are molecular analogues of successful homogeneous catalysts [3–21]. An effective way to obtain such a novel system is the immobilization of a homogeneous transition metal catalyst on an appropriate solid support. The combination of the advantages of conventional homogeneous and heterogeneous catalysis leads to new organic-inorganic hybrid materials, which were successfully applied in asymmetric synthesis, hydrogenation, oxidation and many other reactions [22–28]. Moreover these immobilized catalysts open the pathway to the application of solid-state NMR techniques to the study of the basic steps of hydrogenation reactions, similar to the seminal experiments in liquid state NMR spectroscopy [29–35] and on solid state NMR experiments of neat heterogeneous catalysts [36–39] performed by the Limbach group.

Inorganic porous oxides are the most common materials used as a support for the metal complexes. They are stable over multiple catalytic reaction cycles, inert to the reactants, separable from the reaction media and not harmful to the environment. The discovery of periodic mesoporous silica materials by Mobil Corporation scientists in 1992 was a significant breakthrough in the field of porous materials [40]. This class of materials with MCM- and SBA-type materials as their most prominent representatives offers unprecedented potential for the immobilization of a catalyst [39,41,42]. Their large pore volumes, ordered and tunable pore sizes and their large and relatively homogeneous inner surfaces open up new possibilities for the catalytic conversion of substrates with large molecular size. Due to the presence of surface silanol groups, the physical properties of their inner surface, such as the surface acidity, can be relatively easy chemically modified. Therefore, mesoporous silica materials have gained outstanding importance as solid support in many catalytic reactions.

The chemical modification of the surface silanol groups with anchor groups can be performed in two synthetic routes, namely the grafting method also known as post-synthesis, and the co-condensation, also known as direct synthesis [43,44]. Both routes yield stable surface functionalization that allows successful binding of the metal complexes inside mesopores [43,44].

To optimize efficiency and reproducibility of the immobilized species it is necessary to characterize the structure of metal complexes attached covalently to the silica surface.

The immobilization of the catalyst on an inorganic support combines molecular chemistry with surface science and solid-state chemistry. Due to this complexity a characterization of the metal complexes incorporated onto the silica surface is difficult by classical methods. Therefore, several studies employing advanced spectroscopic techniques such as solid-state NMR were performed to characterize immobilized species on silica surfaces [18–21]. Recently, we reported that a combination of advanced 1D and 2D ^{31}P J-resolved solid-state NMR techniques is able to provide a detailed characterization of the binding situation of Wilkinson's catalyst on the surface of mesoporous silica SBA-3 [45].

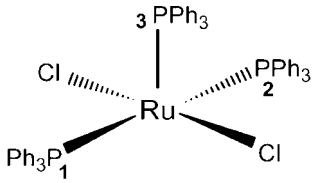

Fig. 1. Structure of the neat ruthenium(II)dichloro(tris)triphenylphosphine ($RuCl_2(PPh_3)_3$) complex (**1**).

The ruthenium(II)dichlorotris(triphenylphosphine) complex (**1**, see Fig. 1) is a prominent catalyst for the reactions of hydrogenation, N-alkylation, transfer hydrogenation of ketones, isomerization of homoallylic alcohols and many others [46]. In its crystalline form this complex has a distorted square pyramidal coordination geometry with a vacant site, where one of the phenyl rings show weak interaction between the *ortho*-H and the Ru center [47]. In solution the three PPh_3-groups exhibit a remarkably complex dynamic behavior, as was originally shown by low-temperature solution NMR experiments of Hoffman and Caulton [48]. Already at relatively low temperatures (−97.5 °C) they observed an A_2X spin-system, where the two phosphorous atoms P_1 and P_2 are chemically equivalent. The corresponding chemical shift values are 24.1 ppm for $A = (P_1, P_2)$, 75.7 ppm for $X = P_3$ and a coupling constant of 30.5 Hz for J(A, X) was measured. Upon increasing temperature a dynamic rearrangement of the PPh_3-groups starts. At room temperature all three phosphorous atoms are rendered chemically equivalent on the NMR time scale and they form an A_3 spin-system with an average isotropic chemical shift of 40.9 ppm. Owing to this, the scalar couplings are no longer observable. From the kinetic analysis of the spectra an activation energy of 10.4 kcal/mol was determined [48]. In the solid-state however, owing to the distortion all three PPh_3-groups are chemically inequivalent. They form an ABX spin-system and are easily resolvable by ^{31}P solid-state MAS NMR spectroscopy as was shown by James and coworkers in studies of neat solid **1** [49]. They found isotropic chemical shifts of P_1: 16.9 ppm, P_2: 22.8 ppm and P_3: 72.5 ppm and a coupling of $J(P_1, P_2) = 333$ Hz. Owing to the resolution of the spectrum they could not resolve the $J(P_{1,2}, P_3)$ couplings.

Immobilized **1** demonstrates high efficiency and stability in many catalytic reactions, even in aqueous media [1]. However, the exact binding of this catalyst to the surface of modified silica materials is not ultimately identified. In the present work we employ a combination of physico-chemical characterization techniques (BET, XRD), advanced ^{31}P solid-state NMR methods and quantum-chemical calculations to shed light into this problem and to develop a detailed binding model of **1** to the inorganic solid support material SBA-3.

2. Experimental

2.1 Materials

All chemicals used for the synthesis were commercially available. The solvents were dried performing standard purifying procedures. All reactions were carried out under an argon atmosphere, using Schlenk techniques.

2.2 Synthesis of $RuCl_2(PPh_3)_3$ (1)

The synthesis follows the route described by Wilkinson *et al.* [50] 1 g of hydrated ruthenium trichloride was dissolved in methanol (250 ml). The reddish brown solution was refluxed for 5 min. After cooling to room temperature, an excess of triphenylphosphine (6 g) was added. The reaction mixture was refluxed for 3 hours under argon and afterwards filtered, washed with diethylether and dried under vacuum.

2.3 Synthesis of mesoporous SBA-3 silica

Mesoporous silica SBA-3 was synthesized as described in Refs. [51,52]. Cetyltrimethylammonium bromide (CTAB) and tetraethyl orthosilicate (TEOS) were used as surfactant and silica source, respectively. The pH-value of the reaction was adjusted by an aqueous solution of 37% HCl. The surfactant, water and hydrochloric acid were mixed for 30 min and then TEOS was added dropwise to this solution. The mixture was stirred at room temperature for 3 hours and the obtained white precipitate was aged for 12 hours. The sample was recovered by filtration and washed with water. After drying at ambient temperature the product was calcinated at 550 °C for 8 h to remove the surfactant.

2.4 Functionalization of SBA-3

The surface of the SBA-3 was functionalized with 3-aminopropyltriethoxysilane (APTES) according to Ref. [22]. First the silica material was activated at 423 K in vacuum for 10 min. Then 3 g of freshly activated SBA-3 were refluxed in toluene (50 ml) with APTES (3 g) for 3 h under argon atmosphere. The resulting solid was washed with diethylether and Soxhlet extracted with anhydrous dichloromethane. Finally it was dried under vacuum for 24 h. From the line-intensities of the directly polarized ^{29}Si-MAS spectrum a surface coverage of the mesopores with APTES linker groups of approximately 24% is estimated following the protocol of Pruski *et al.* [53].

2.5 Immobilization of $RuCl_2(PPh_3)_3$

To a suspension of freshly activated modified silica (1 g) in dry toluene (40 ml), a solution of **1** (0.1 g) in anhydrous toluene (10 ml) was added. The resulting solution was refluxed for 3 h and the obtained solid ($RuCl_2(PPh_3)_x@SiO_2$) was Soxhlet extracted with anhydrous toluene and dried under vacuum for 24 h.

2.6 XRD and BET measurements

The powder X-ray diffraction patterns were collected on a Siemens D5000 diffractometer. Data were collected for 2θ in the range between 1–10 degrees at a scanning rate of 1°/min. The nitrogen adsorption experiments were performed on the Autosorb instrument (Quantachrome Autosorb). Before measurement the known amount of the silica sample was activated in high vacuum at 423 K (623 K for the unmodified silica) for several hours. The BET isotherm, the specific surface area, the pore size diameter and the pore volume were obtained using the program Autosorb.

2.7 Catalytic test experiments

9.5 mg of the $RuCl_2(PPh_3)_x@SiO_2$ catalyst were filled into a Schlenk tube. The catalyst surface was cleaned by evacuating and purging with argon (3x). 2-propanol (5 ml) was added and the mixture was heated at 82 °C for 10 min under argon. Cyclohexanone (0.98 g, 10.0 mmol) was dissolved in 2-propanol (3 ml) and added dropwise to the refluxing mixture. The resulting grey suspension was stirred for 10 min and a solution of NaOH (9.5 mg, 0.237 mmol) in 2-propanol was added dropwise. The mixture was kept at 82 °C for 1 hour. The solid catalyst was removed by filtration and 0.1 ml of the solution was mixed with 0.9 ml of $CDCl_3$ and measured by ^{13}C liquid-state NMR.

2.8 Solid-state NMR experiments

All NMR experiments, except the direct polarized ^{29}Si-MAS measurements, were carried out on a Bruker AVANCE II$^+$ spectrometer at 400 MHz proton resonance frequency, employing a Bruker 4 mm double resonance probe at room temperature.

^{31}P spectra were recorded employing CP-MAS sequences at spinning rates of 10 kHz. Contact times were set to 4 ms. During data acquisition dipolar interactions to protons were decoupled employing tppm decoupling [54] with a 20° phase jump. ^{31}P spectra were referenced to H_3PO_4 as chemical shift standard.

^{31}P J-resolved solid-state NMR spectra were recorded after establishing ^{31}P polarization by means of CP with contact times of 5 ms followed by a rotor synchronized π-pulse after n rotor periods ($n = 1, 2, 3\ldots$) and recording of the spin-echo.

To quantify the surface coverage of the functionalized SBA-3 material, single-pulse directly polarized ^{29}Si-MAS measurements (spectra not shown) were performed on a Varian Infinity Plus Spectrometer at 600 MHz proton resonance frequency, equipped with a Varian triple resonance probe. As an internal reference a special Teflon insert was made and filled with a known quantity of TSP. A single 2 μs pulse with ^1H CW decoupling during acquisition of 512 points and a dwell time of 33.3 μs was used. For deconvolution of the spectra the built-in function of the Spinsight software (Varian) was used.

2.9 Revealing obscured homonuclear scalar couplings by off-magic angle spinning

In contrast to solution, where the phosphorous nuclei P_1 and P_2 of (**1**) are chemically equivalent (see above), in neat crystalline (**1**) they form an AB spin-system with a chemical shift difference of ca. 6 ppm [49]. Since this chemical shift difference is mainly attributed to packing effects it is not evident that in the immobilized catalyst the two phosphorous nuclei are not chemically equivalent. In this case it would be not possible to distinguish them by liquid-state NMR.

The situation is however different in solid-state NMR. As long as the two chemical shift-tensors of P_1 and P_2 are not collinear, the two nuclei are magnetically inequivalent and the CSA creates an effective AX spin-system for most crystallite orientations. Thus the J-interaction between these spins can be in principle revealed. Based on this idea, Wasylishen and coworkers developed special J-resolved solid-state MAS NMR

experiments. A detailed description of these experiments and the underlying theory of detection of J-couplings under magic and off-magic angle spinning conditions is given in a series of seminal papers by Wasylishen and coworkers [55–58] and will not be repeated here. A more general analysis of J-resolved MAS NMR is found in the paper by Levitt and coworkers [59].

Off-magic angle spinning benefits from larger signal to noise ratios and is more robust, compared to dipolar recoupling sequences like PC7, that may suffer from strong signal losses due to insufficient DQ-transfer rates. Likewise, the inadequate sequence, which has to be the refocused type, suffers from signal losses due to the refocusing echo after the DQ conversion.

Furthermore, misadjusted DQ-sequences and absence of coupled spins will result in only noise, in contrast to J-resolved off-MAS NMR, that yields peaks from uncoupled spins, guaranteeing well suited experimental conditions.

In the present paper, J-resolved 2D NMR spectra, recorded under off-MAS conditions, are employed for the detection of possibly obscured ^{31}P-^{31}P J-couplings in the case of immobilized **1**. For the off-MAS J-resolved spectra, the spinning angle was set to approximately 46.7°. All 2D experiments were processed in magnitude mode.

2.10 DFT calculations

Preliminary, quantum chemical calculations were done with the ORCA program system [60] using DFT. All calculations were performed with Becke's three-parameter hybrid functional [61,62] along with the Lee-Yang-Parr correlation functional [63] (B3LYP). For optimizing the structures Pople's double-ζ basis set [64,65] combining d- and p-polarization functions was used for all atoms except Ru, for which an ECP from the Stuttgart group [66] was employed.

As starting structure for neat $RuCl_2(PPh_3)_3$ the X-ray structure published by La Placa *et al.* [47] was utilized. The immobilized catalyst was modeled by substituting one PPh_3 group by ethylamine.

3. Results and discussion

3.1 BET and XRD characterization and catalytic test

3.1.1 BET and XRD

The APTES functionalization of the surface was controlled by means of XRD and BET measurements. For the neat SBA-3 material a specific BET surface of 1120 m^2/g was determined. This surface is reduced by the immobilization of the APTES to 985 m^2/g. A further decrease of the surface area to 830 m^2/g is found after binding the catalyst to the linker. The XRD-spectrum of neat SBA-3 (see ESI, Fig. S1a) reveals a very intense peak assigned to the (100) reflection and two additional peaks with lower intensities attributed to the (110) and (200) reflections. This indicates not only a significant degree of a long range ordering of the structure, but also confirms well formed hexagonal arrays of the mesoporous silica. Upon functionalization of the surface with APTES, a significant shift of the (100) peak towards larger 2θ is observed (see ESI, Fig. S1b) and the

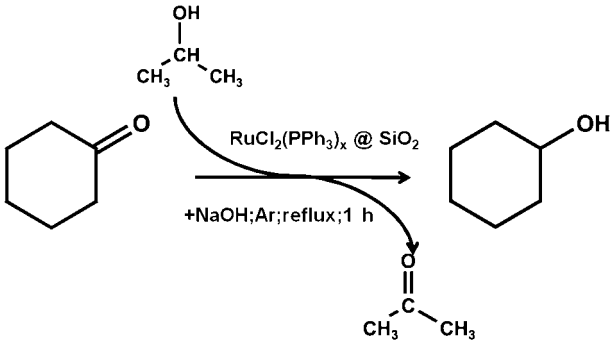

Scheme 1. The transfer hydrogenation of cyclohexanone as test reaction for the catalytic activity.

(110) and (200) reflections are replaced by a broad socket. These measurements show the successful functionalization of the silica surface and also that the mesoporosity of the material is retained.

3.1.2 Catalytic test of the immobilized catalyst

The catalytic activity of the immobilized complex was tested employing the transfer hydrogenation of cyclohexanone to cyclohexanol (see Scheme 1). The resulting spectrum (see ESI, Fig. S2) reveals the signals of both the product cyclohexanol at 70, 35, 23 and 26 ppm, and the substrate cyclohexanone at 211, 41, 27 and 25 ppm.

From the intensity ratio of the C2 carbons (signals at 35 ppm resp. 41 ppm) a reaction turn-over of ca. 52% is estimated.

3.2 Quantum chemical calculations

To the best of our knowledge there are no quantum-chemical calculations of the structure of neat (**1**), despite its importance for hydrogenation reactions and basic science. Since the molecular structure of the catalyst and its linker modified forms are needed for the interpretation of our solid-state NMR data (see below), DFT calculations at the B3LYP/6-31G(d,p) level of theory were performed for both, neat (**1**) and linker modified (**1**). In the case of linker modified (**1**) we were particularly interested to probe, whether the calculations predict magnetic equivalence of P_1 and P_2, if P_3 is replaced by a linker molecule. Such equivalence would render the CSA tensors of P_1 and P_2 collinear and would correspond to a 180° (P_1-Ru-P_2) bond angle.

Starting from the X-ray structure of $RuCl_2(PPh_3)_3$ in a first step the structure optimization was performed (see Fig. 2, structure **I**). In this structure P_1 and P_2 display very similar binding distances to Ru of 2.52 Å and 2.47 Å, respectively, which are much larger than the distance $Ru-P_3$ (2.30 Å). This result is in good agreement with the X-ray data of this complex [47] and confirms the strong low-field shift of P_3 with respect to P_1 and P_2. Moreover this result suggests that the chemical equivalence of P_1 and P_2 in the low-temperature solution NMR spectra of Hoffman and Caulton [48] is probably of dynamical origin, similar to the exchange symmetry of all three phosphorous atoms at RT.

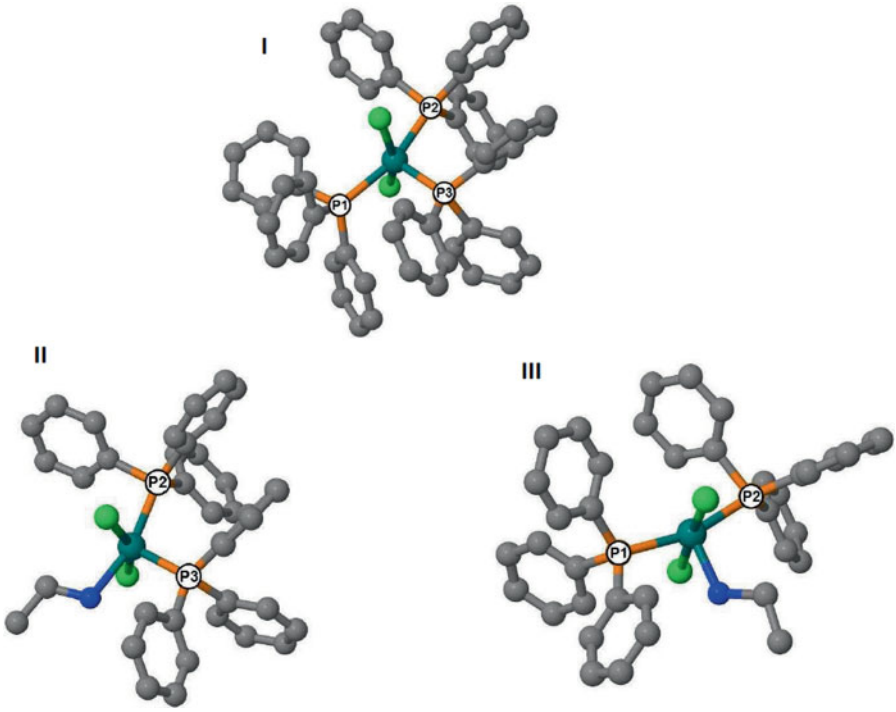

Fig. 2. Optimized structures at the B3LYP/6-31G(d,p) level of neat $RuCl_2(PPh_3)_3$ (**I**), and the model complex for immobilized $RuCl_2(PPh_3)_3$ *via* one amine linker: Replacement of P_1 (**II**) respectively replacement of P_3 (**III**) by ethylamine.

In the second step of the calculations, the binding situation of the immobilized catalyst, where only a single phosphine group is substituted by an APTES linker, was modeled. Since a full DFT calculation of a silica bound APTES linker to the ruthenium is not feasible, we had to choose a suitable calculational model. Assuming that only the atoms in the first three coordination spheres have a strong influence on the electronic environment, we chose ethylamine as simplest model for the silica bound linker. Ethylamine models both the amine function and the alkyl chain of the APTES linker. Using this model we studied the binding geometry of the phosphines. Two different situations were considered, namely that either phosphine P_1 or P_3 was replaced by an ethylamine ligand.

Substitution of P_1 by ethylamine yields the structure with the lower energy. In the optimized structure **II**, the binding distances Ru−P_2 and Ru−P_3 slightly changed compared to **I** (see Table 1) but there is still a relatively large gap of approximately 0.1 Å between these two distances. This would imply a chemical and magnetic inequivalence of the two phosphorous atoms and an observable chemical shift difference in the ^{31}P solid-state NMR of immobilized $RuCl_2(PPh_3)_3$ in the case of substitution of only one phosphine.

Substitution of P_3 by ethylamine yields a structure with higher energy (see Fig. 2, structure **III**) where the binding situation of the two remaining phosphines is differ-

Table 1. Selected bond lengths and bond angles of model complexes for neat $RuCl_2(PPh_3)_3$ (**I**) and immobilized $RuCl_2(PPh_3)_3$ (**II** and **III**) optimized at the B3LYP/6-31G(d,p) level of theory.

structure	bond lengths in Å		bond angles in degree	
I	$Ru-P_1$	2.52	P_1-Ru-P_2	158.4
	$Ru-P_2$	2.47	P_1-Ru-P_3	100.0
	$Ru-P_3$	2.30	P_2-Ru-P_3	100.8
II	$Ru-P_2$	2.39	P_2-Ru-P_3	103.6
	$Ru-P_3$	2.28		
III	$Ru-P_2$	2.45	P_1-Ru-P_2	162.9
	$Ru-P_1$	2.42		

ent. The bond lengths $Ru-P_1$ and $Ru-P_2$ are very similar (see table). Thus, these two phosphines could be chemically equivalent, however, since the bond angle P_1-Ru-P_2 ($\approx 163^\circ$) strongly differs from 180°, they are magnetically inequivalent, which means that their scalar coupling should be observable in solid-state NMR.

3.3 Solid-state NMR

3.3.1 1D and 2D ^{31}P solid-state NMR experiments on the neat catalyst

The presence of three PPh_3-ligands coordinated to the metal center allows employing ^{31}P NMR methods as an efficient tool to characterize the structure of the ruthenium catalyst before and after immobilization on the solid support.

The ^{31}P CP-MAS spectrum of neat **1** in Fig. 3a and b exhibits the signals assigned to the three phosphorous atoms of the nonequivalent triphenylphosphine ligands. We observed two doublets at 16 and 32 ppm assigning the *trans*-phosphines P_1 and P_2, respectively, and one narrow signal at 75 ppm which is attributed to the phosphine ligand P_3, on top of the distorted square pyramid. This result slightly differs from the data reported previously by Mac Farlane [49], who detected a smaller chemical shift difference between P_1 and P_2 of only 6 ppm instead of 16 ppm found by us. This difference can be caused by two reasons, which are not mutually exclusive. On the one hand our spectra were recorded at a higher field 161.75 MHz (9.4 Tesla), which yields a higher resolution. On the other hand, such small variations in the chemical shift are also indicative of crystallization effects or polymorphic behavior.

The splitting of the two signals at the high field side of the spectrum arises from the $^2J(P,P)$-coupling between P_1 and P_2 phosphorous atoms, with a 300 Hz J-coupling constant.

The heteronuclear spin interactions between the two NMR active Ru isotopes and the ^{31}P nuclei are visible as an asymmetric foot of satellite lines around the isotropic peak at 75 ppm in the spectrum, overlapping with the spinning sidebands of the doublet at 16 ppm (see Fig. 3b).

(Ru, P) J-couplings in solid Ru-Phosphine complexes were first described and analyzed in detail by Eichele *et al.* [67]. Following their analysis, the observed satellite

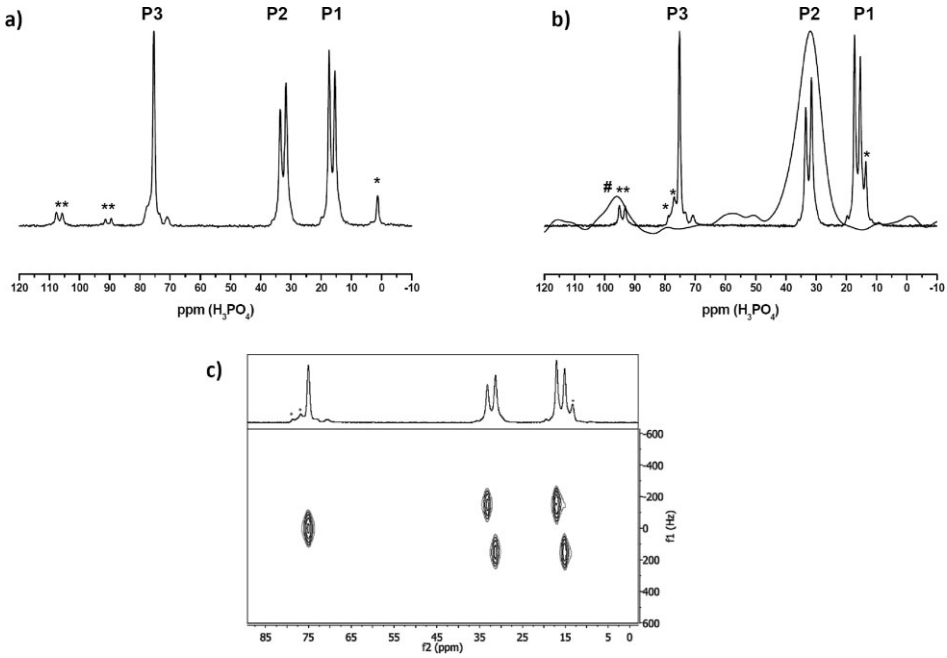

Fig. 3. a) ^{31}P CP-MAS spectrum of **1** before immobilization at 12 kHz spinning speed. **b)** ^{31}P CP-MAS spectrum of **1** before and after its immobilization on the mesoporous silica at 10 kHz spinning speed. **c)** ^{31}P 2D J-resolved NMR spectrum of neat **1** (spinning speed 10 kHz). *Note:* Spinning side-bands of **1** are denoted by asterisks, spinning side-bands of the immobilized catalyst are denoted by #.

pattern is attributed to $^{1}J(^{99}Ru,^{31}P)$ coupling. $^{1}J(^{101}Ru, ^{31}P)$ coupling is absent probably due to self-decoupling effects which refers to the 5.8 times higher quadrupolar moment of ^{101}Ru with respect to ^{99}Ru [67].

In the next step the 2D J-resolved ^{31}P NMR spectrum of **1** was measured (see Fig. 3c). It allows the precise determination of the number of bound phosphine ligands in the investigated sample, based on the analysis of the ^{31}P spin-spin interactions in the molecule. Only the well-resolved pattern of homonuclear J-coupling due to interactions between P_1 and P_2 phosphorus nuclei is visible along the f_1 dimension. This clearly supports the results of the 1D ^{31}P CP-MAS experiments about the spin-spin interaction pattern of **1**.

3.3.2 ^{29}Si and ^{13}C solid-state NMR of the immobilized catalyst

To verify the successful immobilization, ^{13}C and ^{29}Si CP-MAS spectra were recorded (see Fig. 4). The ^{29}Si CP-MAS spectrum (Fig. 4a) clearly proofs the presence of the linker molecules on the SBA-3 surface after immobilization by the presence of ^{29}Si T-peaks between −50 and −75 ppm. In accordance with the presence of ^{13}C peaks at 128 ppm (Fig. 4b), associated with the PPh_3 of the $RuCl_2(PPh_3)_3$ complex, the binding of $RuCl_2(PPh_3)_3$ to the linker molecules is clearly proofed.

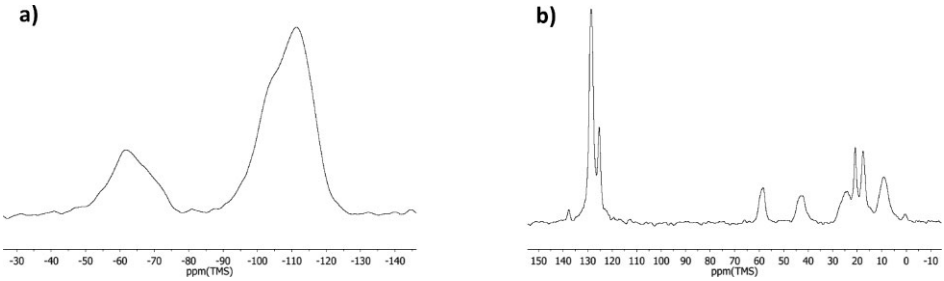

Fig. 4. a) ^{29}Si CP-MAS Spectrum of the mesoporous silica after immobilization at 5 kHz spinning speed. **b)** ^{13}C CP-MAS spectrum after immobilization at 10 kHz spinning speed.

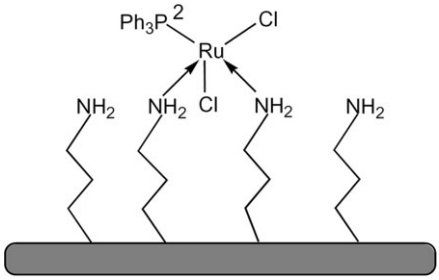

Fig. 5. Sketch of the immobilization of **1** at the surface of amine modified silica material SBA-3.

3.3.3 1D and 2D ^{31}P solid-state NMR experiments on the immobilized catalyst

After immobilization of **1** on the functionalized surface of the SBA-3 material, the ^{31}P CP-MAS spectrum has significantly changed (see Fig. 3b). The peaks attributed to the phosphine ligands with phosphorous atoms labeled as P_1 and P_3 are no longer visible in the spectrum. Instead only one broad signal at 32 ppm, *i. e.* the position of phosphine ligand P_2 is visible.

The presence of a single signal not only confirms the successful reaction of **1** but also suggests that the two phosphine ligands were replaced by the amine groups of the APTES linker bound to the surface. Thus, the heterogenized catalyst appears to be attached to the surface through two organic linkers (see Fig. 5).

To probe whether really two PPh_3 groups were replaced by linkers, we employed J-resolved 2D solid-state NMR experiments. Since fast spinning MAS experiments are not able to resolve two chemically equivalent nuclei, [45] a fast spinning off-magic angle J-resolved experiment was conducted, which is able to resolve possibly obscured ^{31}P-^{31}P J-couplings.

The ^{31}P 2D J-resolved off-MAS spectrum of immobilized **1** is shown in Fig. 6. In the spectrum there is evidently no visible J-coupling. This result supports our hypothesis of the absence of two equivalent phosphorous ligands. However, it has to be also ensured that the immobilization of the catalyst has not caused an accidental

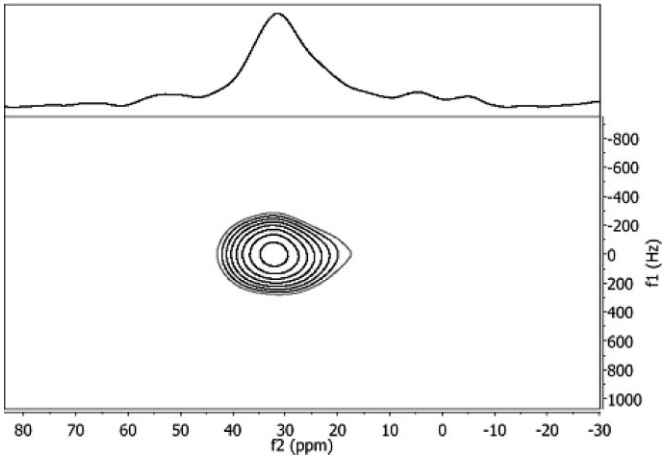

Fig. 6. Two dimensional ^{31}P J-resolved off-MAS spectrum of immobilized **1**.

magnetically equivalence of the ^{31}P nuclei in the phosphine groups, leading to an A_2 spin-system with invisible spin-spin coupling.

Since the preliminary quantum chemical calculations described above clearly show that for mono-ethylamine substituted (**1**) even in the gas-phase the two phosphines are magnetically inequivalent, we conclude that indeed two phosphines are replaced by the linker.

This conclusion is further supported by the broad line-width of the ^{31}P spectrum of the immobilized catalyst. Magnetic equivalence is tantamount to a highly ordered state, which corresponds to relatively narrow lines, similar to the neat crystalline phase. However, even without any applied apodization, the phosphorous line is approximately 1 kHz wide. From the J-resolved, rotor synchronized spin-echo experiment, where single spectra are recorded every 200 μs, a T_2 time of 10 ms can be approximated, which corresponds to a homogenous line broadening of ca 30 Hz which is at least one order smaller than the observed one. Thus, the broadening of the ^{31}P line is inhomogeneous and the system exhibits a very high degree of static disorder.

4. Summary and conclusions

The Ruthenium (II) catalyst $RuCl_2(PPh_3)_3$ was immobilized on the surface of mesoporous silica material SBA-3, modified with 3-aminopropyltriethoxysilane linkers. To characterize the exact binding of the ruthenium complex to the solid support, a combination of 1D and 2D ^{31}P solid-state NMR techniques were applied. Quantum chemical calculations were performed to elucidate the structure of two ruthenium catalyst/linker scenarios under perfect condition. The first results of these calculations yield magnetically inequivalent ^{31}P nuclei for the scenarios, approving the utilization of 2D off-magic angle NMR.

The results of ^{31}P CP-MAS experiments not only confirmed the attachment of the catalyst to the organic linker but also suggest coordination to the surface through two organic linker molecules coordinated to the metal center. The 2D ^{31}P J-resolved off-magic angle experiments did not show cross peaks of J-coupled phosphines, and thus reveal the number of phosphine groups present in the immobilized complex. There is clear evidence that two phosphine ligands of $RuCl_2(PPh_3)_3$ are exchanged by amine groups of the linker molecules.

The presented results provide new insights into the structure of heterogenized ruthenium catalysts. These insights can help understanding the activity and stability of this catalyst in the catalytic reactions. Finally, it is clearly shown that the application of advanced ^{31}P solid-state NMR techniques combined with quantum-chemical calculations allows not only the detection, but also the characterization of transition metal phosphine complexes immobilized on support surfaces on the molecular level.

For the complete understanding of phosphine bindings and dynamics in $RuCl_2(PPh_3)_3$ containing catalyst systems advanced quantum chemical calculations at a higher level of theory including relativistic effects are mandatory. These investigations have to be combined with low temperature liquid-state NMR, in order to probe whether the phosphine ligands P_1 and P_2 are indeed chemically equivalent at low temperatures. These studies are beyond the scope of the present paper.

Acknowledgement

Financial support of the Deutsche Forschungsgemeinschaft under contract Bu-911-12/2 and the state of Hessia in the frame-work of LOEWE SOFT-CONTROL are gratefully acknowledged.

References

1. H. X. Li, F. Zhang, H. Yin, Y. Wan, and Y. F. Lu, Green Chem., **9** (2007) 500.
2. J. Guzman and B. C. Gates, Dalton T. (2003) 3303.
3. H. Brunner, E. Bielmeier, and J. Wiehl, J. Organomet. Chem. **384** (1990) 223.
4. B. E. Handy, I. Gorzkowska, J. Nickl, A. Baiker, M. Schramlmarth, and A. Wokaun, Ber. Bunsen-Ges. Phys. Chem. **96** (1992) 1832.
5. H. Werner and U. Mohring, J. Organomet. Chem. **475** (1994) 277.
6. J. Bluemel, Ber. Bunsen-Ges. Phys. Chem. **99** (1995) 1343.
7. J. U. Koehler and H. L. Krauss, J. Mol. Catal. **A 123** (1997) 49.
8. J. Evans, A. B. Zaki, M. Y. El-Sheikh, and S. A. El-Safty, J. Phys. Chem. B **104** (2000) 10271.
9. A. J. Sandee, J. N. H. Reek, P. C. J. Kamer, and P. W. N. M. van Leeuwen, J. Am. Chem. Soc. **123** (2001) 8468.
10. J. K. Lee, T. J. Yoon, and Y. K. Chung, Chem. Comm. (2001) 1164.
11. W. H. Cheung, W. Y. Yu, W. P. Yip, N. Y. Zhu, and C. M. Che, J. Org. Chem. **67** (2002) 7716.
12. R. Becker, H. Parala, F. Hipler, O. P. Tkachenko, K. V. Klementiev, W. Grünert, H. Wilmer, O. Hinrichsen, A. Birkner, M. Muhler, C. Wöll, S. Schäfer, and R. A. Fischer, Angew. Chem. Intl. Ed. **43** (2004) 2839.
13. J. O. Krause, O. Nuyken, K. Wurst, and M. R. Buchmeiser, Chem.-Eur. J. **10** (2004) 777.
14. A. Crosman and W. E. Hoelderich, J. Catal. **232** (2005) 43.
15. A. M. J. Rost, H. Schneider, J. P. Zoller, W. A. Herrmann, and F. E. Kuhn, J. Organomet. Chem. **690** (2005) 4712.
16. M. Hartmann and C. Streb, J. Porous Mat. **13** (2006) 347.

17. X. S. Zhao, X. Y. Bao, W. Guo, and F. Y. Lee, Mater. Today **9** (2006) 32.
18. T. Posset and J. Bluemel, J. Am. Chem. Soc. **128** (2006) 8394.
19. J. W. Wiench, Ch. Michon, A. Ellern, P. Hazendonk, A. Iuga, R. Angelici, and M. Pruski, J. Am. Chem. Soc. **131** (2009) 11801.
20. J. R. Rapp, Y. Huang, M. Natella, Y. Cai, V. S. Y. Lin, and M. Pruski, Solid State NMR **35** (2009) 2.
21. K. Mao, J. W. Wiench, V. S. Y. Lin, and M. Pruski, J. Magn. Reson. **196** (2009) 1.
22. T. Joseph, S. S. Deshpande, S. B. Halligudi, A. Vinu, S. Ernst, and M. Hartmann, J. Mol. Catal. **A 206** (2003) 13.
23. L. Huang, J. Chun, and S. Kawi, React. Kinet. Catal. Lett. **82** (2004) 65.
24. L. Huang and S. Kawi, Catal. Lett. **90** (2003) 165.
25. L. Huang and S. Kawi, Catal. Lett. **92** (2004) 57.
26. S. W. Song, K. Hidajat, and S. Kawi, Langmuir **21** (2005) 9568.
27. V. Dufaud, F. Beauchesne, and L. Bonneviot, Angew. Chem., Int. Ed. **44** (2005) 3475.
28. E. Duliere, M. Devillers, and J. Marchand-Brynaert, Organometallics **22** (2003) 804.
29. B. Chaudret, H. Limbach, and C. Moise, Comptes rendus de l'Académie des sciences. Série 2, Mécanique, Physique, Chimie, Sciences de l'univers, Sciences de la Terre **315** (1992) 533.
30. H. H. Limbach, G. Scherer, M. Maurer, and B. Chaudret, Angew. Chem. Int. Ed. Engl. **31** (1992) 1369.
31. H. H. Limbach, G. Scherer, L. Meschede, Aguilar-F. Parrilla, B. Wehrle, J. Braun, C. Hoelger, H. Benedict, G. Buntkowsky, W. P. Fehlhammer, J. Elguero, J. A. S. Smith, and B. Chaudret, *Ultrafast Reaction Dynamics and Solvent Effects, Experimental and Theoretical Aspects*, Y. Gauduel and P. J. Rossky (Eds.), American Inst. of Physics, (1993) 225.
32. S. Gründemann, H.-H. Limbach, V. Rodriguez, B. Donnadieu, S. Sabo-Etienne, and B. Chaudret, Ber. Bunsen-Ges. Phys. Chem. **102** (1998) 344.
33. H.-H. Limbach, S. Ulrich, S. Gründemann, G. Buntkowsky, S. Sabo-Etienne, B. Chaudret, G. J. Kubas, and J. Eckert, J. Am. Chem. Soc. **120** (1998) 7929.
34. S. Gründemann, H.-H. Limbach, G. Buntkowsky, S. Sabo-Etienne, and B. Chaudret, J. Phys. Chem. A **103** (1999) 4752.
35. J. Matthes, S. Gründemann, A. Toner, Y. Guari, B. Donnadieu, J. Spandl, S. Sabo-Etienne, E. Clot, H. H. Limbach, and B. Chaudret, Organometallics **23** (2004) 1424.
36. F. Wehrmann, T. Fong, R. H. Morris, H.-H. Limbach, and G. Buntkowsky, Phys. Chem. Chem. Phys. **1** (1999) 4033.
37. J. Matthes, T. Pery, S. Gründemann, G. Buntkowsky, B. Sabo-Etienne, B. Chaudret, and H. H. Limbach, J. Am. Chem. Soc. **126** (2004) 8366.
38. T. Pery, K. Pelzer, G. Buntkowsky, K. Philippot, H. H. Limbach, and B. Chaudret, Chem. Phys. Chem. **6** (2005) 605.
39. A. Adamczyk, Y. Xu, B. Walaszek, F. Roelofs, T. Pery, K. Pelzer, K. Philippot, B. Chaudret, H.-H. Limbach, H. Breitzke, and G. Buntkowsky, Top Catal. **48** (2008) 75.
40. C. T. Kresge, M. E. Leonowicz, W. J. Roth, J. C. Vartuli, and J. S. Beck, Nature **359** (1992) 710.
41. D. Y. Zhao, Q. S. Huo, J. L. Feng, B. F. Chmelka, and G. D. Stucky, J. Am. Chem. Soc. **120** (1998) 6024.
42. X. S. Zhao and G. Q. Lu, J. Chem. Phys. **102** (1998) 1556.
43. F. Hoffmann, M. Cornelius, J. Morell, and M. Froba, Angew. Chem., Int. Ed. **45** (2006) 3216.
44. A. Stein, B. J. Melde and R. C. Schroden, Adv. Mater. **12** (2000) 1403.
45. A. Gruenberg, Y. P. Xu, H. Breitzke, and G. Buntkowsky, Chem.-Eur. J. **16** (2010) 6993.
46. S. Komiya, *Synthesis of Organometallic Compounds*. Wiley (1997).
47. S. J. La Placa and J. A. Ibers, Inorg. Chem. **4** (1965) 778.
48. P. Hoffman and K. Caulton, J. Am. Chem. Soc. **97** (1975) 4221.
49. K. S. MacFarlane, A. M. Joshi, S. J. Rettig, and B. R. James, Inorg. Chem. **35** (1996) 7304.
50. P. S. Hallman, T. A. Stephenson, and G. Wilkinson, *Inorg. Synth.* R. W. Parry (Ed.), John Wiley & Sons, Inc., Hoboken, NJ, USA (1970) Vol. 12.
51. M. Mesa, L. Sierra, and J. L. Guth, Microporous Mesoporous Mater. **102** (2007) 70.

52. O. A. Annunziata, A. R. Beltramone, M. L. Martinez, and L. L. Belar, J. Coll. Surf. Sci. **315** (2001) 184.
53. S. Huh, J. W. Wiench, J.-C. Yoo, M. Pruski, and V. S.-Y. Lin, Chem. Mater. **15** (2003) 4247.
54. A. E. Bennett, C. M. Rienstra, M. Auger, K. V. Lakshmi, and R. G. Griffin, J. Chem. Phys. **103** (1995) 6951.
55. G. Wu and R. E. Wasylishen, Organometallics **11** (1992) 3242.
56. G. Wu and R. E. Wasylishen, J. Chem. Phys. **98** (1993) 6138.
57. G. Wu and R. E. Wasylishen, J. Chem. Phys. **100** (1994) 5546.
58. G. Wu and R. E. Wasylishen, Inorg. Chem. **35** (1996) 3113.
59. L. Duma, W. C. Lai, M. Carravetta, L. Emsley, S. P. Brown, M. H. Levitt, Chem. Phys. Chem. **5** (2004) 815.
60. F. Neese, Wiley Interdisciplinary Reviews-Computational Molecular Science **2** (2012) 73.
61. A. D. Becke, J. Chem. Phys. **98** (1993) 1372.
62. A. D. Becke, J. Chem. Phys. **98** (1993) 5648.
63. C. T. Lee, W. T. Yang, and R. G. Parr, Phys. Rev. B **37** (1988) 785.
64. C. Harihara and J. A. Pople, Theor. Chim. Acta **28** (1973) 213.
65. W. J. Hehre, R. Ditchfield, and J. A. Pople, J. Chem. Phys. **56** (1972) 2257.
66. D. Andrae, U. Haussermann, M. Dolg, H. Stoll, and H. Preuss, Theor. Chim. Acta. **77** (1990) 123.
67. K. Eichele, R. E. Wasylishen, J. F. Corrigan, S. Doherty, Y. Sun, and A. J. Carty, Inorg. Chem. **32** (1993) 121.